# Synergistic Effect of Metal Cations and Visible Light on 2D $MoS_2$ Nanosheet Aggregation

Manuscript submitted to

*Environmental Science & Technology*

Bei Liu,[a] Qi Han,[a] Li Li,[a] Sunxiang Zheng,[b] Yufei Shu,[a] Joel A. Pedersen,[c]
Zhongying Wang[a*]

[a] School of Environmental Science and Engineering, Southern University of Science and Technology, Shenzhen 518055, China
[b] Andlinger Center for Energy and the Environment, Princeton University, Princeton, New Jersey 08544, USA
[c] Departments of Soil Science, Civil & Environmental Engineering, and Chemistry, University of Wisconsin, Madison, Wisconsin 53706, USA

---

[*] to whom correspondence should be addressed. e-mail: wangzy6@sustech.edu.cn; tel.: +86-075588018040;

## ABSTRACT

Aggregation significantly influences the transport, transformation, and bioavailability of engineered nanomaterials. Two-dimensional $MoS_2$ nanosheets are one of the most well-studied transition metal dichalcogenide nanomaterials. Nonetheless, the aggregation behavior of this material under environmental conditions is not well understood. Here, we investigated the aggregation of single-layer $MoS_2$ (SL-$MoS_2$) nanosheets under a variety of conditions. Trends in the aggregation of SL-$MoS_2$ are consistent with classical DLVO colloidal theory, and the critical coagulation concentrations of cations follow the order of trivalent ($Cr^{3+}$) < divalent ($Ca^{2+}$, $Mg^{2+}$, $Cd^{2+}$) < monovalent cations ($Na^+$, $K^+$). Notably, $Pb^{2+}$ and $Ag^+$ destabilize $MoS_2$ nanosheet suspensions much more strongly than do their divalent and monovalent counterparts. This effect is attributable to Lewis soft acid–base interactions of the cations with $MoS_2$. Visible light irradiation synergistically promotes the aggregation of SL-$MoS_2$ nanosheets in the presence of cations, which was evident even in the presence of natural organic matter. The light-accelerated aggregation was ascribed to dipole–dipole interactions due to transient surface plasmon oscillation of electrons in the metallic 1T phase, which decrease the aggregation energy barrier. These results reveal the phase-dependent aggregation behaviors of engineered $MoS_2$ nanosheets with important implications for environmental fate and risk.

## Synopsis

Aggregation behavior of $MoS_2$ nanosheets was comprehensively explored as influenced by environmental factors including nature of cations, light irradiation and natural organic matter.

## Keywords

2D nanomaterials, molybdenum disulfide, environmental behavior, aggregation and sedimentation, visible light

49 **Table of Contents (TOC) and Abstract Art**

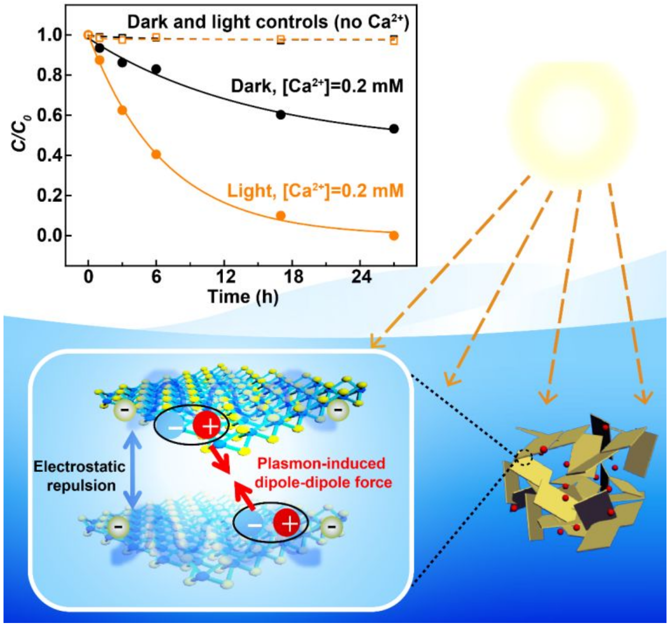

50

# INTRODUCTION

Transition metal dichalcogenides (TMDCs; with the formula $MX_2$, where M is a transition metal from group IV, V or VI, and X is chalcogen) rank among the most promising types of next-generation two-dimensional nanomaterials. Chemical, mechanical or ultrasonic exfoliation methods allow formation of monolayer or few-layer TMDCs from their bulk crystals.[1,2] Molybdenum disulfide ($MoS_2$), a typical TMDC consisting of covalently bonded atomic trilayers of sulfur-molybdenum-sulfur, has been the most intensely investigated 2D material beyond graphene and has demonstrated applications in electronics,[3] biomedical,[4] catalysis,[5,6] and energy-related fields.[7] Owing to their unique properties such as atomic thinness, suitable band gap, and high affinity for heavy metals, $MoS_2$ nanosheets show considerable promise in environmental applications such as membrane separation,[8] photocatalysis,[9] disinfection,[10] and heavy metal remediation.[11–13] The intensive research and potential applications of $MoS_2$ nanosheets point toward their increasing use and inevitable subsequent release to aquatic environments, and thus a thorough understanding of their fate, transformation and risks as assessment at early stage of development is imperative.

Aggregation represents one of the most important processes influencing the environmental behavior of nanomaterials. In the course of aggregation, dispersed nanomaterials assemble into flocs, which decreases the “available” reactive surface area, thus can ultimately affect nanomaterial mobility, degradation,[14,15] bioavailability and toxicity to aquatic organisms.[16–19] The aggregation behavior of 2D nanosheets may also be important in the assembly of 3D macrostructures.[20] Recently, the aggregation and sedimentation of 2D nanomaterials including graphene oxide (GO), black phosphorus, and titanium carbide (MXene) nanosheets have been reported, [21–24] revealing the influence of environmental factors (*i.e.,* cation species and concentration, natural organic matter) on the aggregation rate and environmental outcomes. Similar to these 2D nanomaterials, $MoS_2$ suspensions exhibit colloidal instability and inhibited transport in the presence of hard metal cations (*viz.* $Na^+$, $K^+$, and $Ca^{2+}$) or under extremely acidic conditions due to charge screening decreasing electrostatic repulsion between nanosheets.[25–27] Prior studies compared mono- and divalent hard metal cations, with the conclusion consisting with the Schulze-Hardy rule.[25,27] However, the sulfur atoms on $MoS_2$ nanosheets are soft Lewis bases, which exhibit stronger affinity for soft Lewis acids (*e.g.*, $Pb^{2+}$) relative to hard ones (*e.g.*, $Ca^{2+}$, $Mg^{2+}$).[28] Consequently, $MoS_2$ nanosheets are expected to exhibit ion-specific in addition to the valence-dependent aggregation behaviors that could be predicted by the Schulze-Hardy rule. Until now, colloidal stability of $MoS_2$ as a function of cation electronegativity has not been examined. Our hypothesis is that soft metal cations would interact more strongly with the S atoms of $MoS_2$ nanosheets and therefore be more effective in destabilizing them.

Another unique property possibly related to aggregation is that $MoS_2$ nanosheets are photoactive and subject to light-induced transformations.[10,29] Notably, $MoS_2$ mainly exists in two crystal structures depending on the atom-stacking configurations: the semiconducting 2H phase (trigonal prismatic) and the metallic 1T phase (octahedral).[30,31] The bandgap energy ($E_g$) of semiconducting 2H-$MoS_2$ depends on the number of stacked $MoS_2$ monolayers and increases from 1.29 eV (i.e., 653 nm) for bulk $MoS_2$ to ~1.9 eV (i.e., ~961 nm) for single-layer $MoS_2$.[32] The strong increase in $E_g$ as crystal thickness decreases beyond 100 nm is due primarily to confinement-induced increase in the indirect bandgap.[32] For the 2H-$MoS_2$ phase, supra-bandgap illumination allows electron–hole separation, which can drive photochemical reactions.[10,18] Compared to the 2H phase, the metastable, metallic 1T phase possess a higher concentration of free charge carriers and with sufficient Li or K doping can achieve surface plasmon resonance under visible and near

UV range.[33,34] Such photoactive properties have promised the environmental behaviors of $MoS_2$ including aggregation are susceptible to illumination. Numerous studies have reported that light-irradiation can alter aggregation behaviors of nanomaterials by initiating redox reactions ($As_2S_3$),[35] removing surface groups or coatings (carbon nanotubes,[36,37] GO,[38] $TiO_2$[39]), or inducing surface plasmon oscillation (Ag, Au).[40–42] For $MoS_2$, long-term light exposure can reduce the surface charge through redox reactions and thus destabilize the nanosheet.[18] Until now, however, the effect of light irradiation on the initial aggregation of pristine $MoS_2$ nanosheets remains unexplored. Such information is critical to understanding the dispersion and lifetime of engineered $MoS_2$ nanosheets in the photocatalytic applications, as well as understanding the environmental fate, transport potential, nanosheet reactivity and toxicity upon sunlight irradiation in the natural environment.

In the present study, single-layer $MoS_2$ (SL-$MoS_2$) nanosheets without any coatings were prepared *via* chemical exfoliation and extensively characterized to determine their chemical composition, morphology, and surface chemistry. Aggregation kinetics of $MoS_2$ nanosheets were measured using time-resolved dynamic light scattering (TRDLS) in the presence of mono-, di-, and trivalent cations. The effects of visible light irradiation on aggregation were explored and mechanisms involved in the photoinduced process were discussed. Finally, light- and cation-induced aggregation was examined in the presence of natural organic matter (NOM). This detailed study advances the understanding of the fate of $MoS_2$ nanosheets under environmental conditions.

## MATERIALS AND METHODS

**Synthesis and Characterization of $MoS_2$ Nanosheets.** Chemicals and their purities and supplies are reported in the Supporting Information. A dispersion of SL-$MoS_2$ nanosheets containing a mixture of 1T and 2H phases was prepared by organolithium intercalation of $MoS_2$

powder followed by forced hydration as described in our previous study.[43] A detailed description of the synthesis approach is given in the Supporting Information. Semiconducting $MoS_2$ (referred to as 2H-$MoS_2$) was obtained by pressurized hydrothermal treatment of the exfoliated SL-$MoS_2$ in $N_2$.[44] Specifically, 20 mL of a ~500 mg/L SL-$MoS_2$ suspension was deoxygenated in a $N_2$-filled glove box, added to a Teflon-lined autoclave (50 mL volume, Wenbo Experimental Instrument Co., Ltd), and subjected to the hydrothermal treatment at 200 °C for 2 h.

The morphologies of pristine SL-$MoS_2$ nanosheets, 2H-$MoS_2$ nanosheets, and their aggregates were characterized by transmission electron microscopy (TEM; FEI Talos F200X microscope equipped with a Schottky emitter gun operated at 200 kV), scanning electron microscopy (SEM; Zeiss Merlin), and atomic force microscopy (AFM; MFP-3D-Stand Alone, Asylum Research). We performed X-ray photoelectron spectroscopy (XPS) survey and high-resolution scans with a PHI 5000 Versaprobe III equipped with a monochromatic Al anode (Al Kα = 1486.7 eV) as X-ray source. The powder X-ray diffraction (XRD) pattern was collected on a Rikagu Smartlab diffractometer (Cu Kα = 1.54 Å). Apparent zeta potentials were determined from electrophoretic mobilities (Nanosizer, NanoBrook Omni, Brookhaven, U.S.A.) from three replicate samples and three measurements for each with 20 cycles. UV-visible absorption spectra of the dispersed $MoS_2$ nanosheets were obtained by ultraviolet-visible spectrophotometer (UV-vis, Bluestar, LabTech). The total concentration of SL-$MoS_2$ prior to aggregation was accurately determined by digestion in a 0.2 M $HNO_3$ and 0.5 M $H_2O_2$ solution, followed by measurement of the soluble Mo concentration by inductively coupled plasma–optical emission spectrometer (ICP-OES, iCAP 7400, Thermo Scientific).

**Aggregation Kinetics.** A SL-$MoS_2$ suspension was prepared by diluting an aliquot of the exfoliated $MoS_2$ stock solution in water buffered to pH 5 with 10 mM sodium acetate (the sodium acetate contributed 6.5 mM $Na^+$ to the solution and did not induce measurable aggregation). Time-resolved DLS was used to measure the aggregation kinetics of $MoS_2$ nanosheet suspensions, and the *z*-averaged hydrodynamic diameter ($D_h$) of $MoS_2$ nanosheets was monitored as a function of time in solutions of the nitrate salts of $K^+$, $Na^+$, $Ag^+$, $Ca^{2+}$, $Mg^{2+}$, $Cd^{2+}$, $Pb^{2+}$, and $Cr^{3+}$ over a wide range of cation concentrations (viz. 0.02-50 mM). The speciation of cations as a function of pH was determined by Visual Minteq. All of these cations exist primarily as unhydrolyzed cations at the pH of our experiments except $Cr^{3+}$, which is present as $Cr_3(OH)_4^{5+}$, $Cr_2(OH)_2^{4+}$, $Cr^{3+}$, $CrOH^{2+}$, $Cr(OH)_2^+$, $Cr(OH)_3$ at pH 5 (Figure S1). Based on the speciation of chromium (III) under our experimental conditions, we used an average valence of 2.82 in calculations. Measurements were made every 30 s for 30 min. Attachment efficiencies (α) — the ratio between the rates of slow (reaction-limited regime in the presence of energy barrier) to fast aggregation (diffusion-limited regime in the absence of energy barrier) — were obtained by normalizing the initial slope of the aggregation profile at each concentration by that in the fast regime:[22]

$$\alpha = \frac{k_a}{k_{a,\,fast}} = \frac{\frac{1}{N_0}\left(\frac{D_h(t)}{dt}\right)_{t\to 0}}{\frac{1}{N_{0,fast}}\left(\frac{D_h(t)}{dt}\right)_{t\to 0,fast}}$$

where the $k_a$ are the initial aggregation rate constants, which are proportional to the initial rate of $D_h$ increase with time, and $N_0$ is the initial SL-$MoS_2$ concentration (~10 mg/L in all samples). For slow aggregation at relatively low cation concentrations (i.e., up to 2−20 mM $Na^+$) the slope of the initial linear region was determined from the $D_h$ versus time plot over 30 min. For the fast aggregation, the slope was determined from the first recording to an average $D_h$ of 1400 nm within 30 min, the range which could assure a good linear regression ($R^2 > 0.9$). The critical coagulation concentrations (CCC) was determined for each cation from the intersection of extrapolated lines through the diffusion- and reaction-limited regimes. Influence of NOM on the aggregation kinetics was determined by the addition of Suwannee River NOM (SRNOM) as described in Text S3.

**Visible Light Illumination Experiments.** Visible light illumination experiments were performed in a PCX50C Discover multi-channel parallel photocatalytic reaction system (Perfect Light Co., Ltd.) with a 5 W white LED light (400 nm ≤ λ ≤ 800 nm). The light intensity is adjustable with maximum irradiation intensity of 100 $mW/cm^2$, which is comparable to the annual global average intensity of natural sunlight.[45] The SL-$MoS_2$ dispersion (30 mL) was spiked with the desired concentration of cations and was transferred into the cylindrical quartz tubes of the reactor. The typical light intensity of 100 $mW/cm^2$ and a concentration of 2 mM $Ca^{2+}$ was used in all the irradiation experiments unless noted. During the irradiation process, the temperature of the reactor was kept at 25 °C with an electronic fan, and measured with a thermometer after the experiments. Optical absorbance at 450 nm was used to quantitatively describe the evolution of the suspension concentration and the extent that $MoS_2$ aggregates sedimented, as the Beer-Lambert law is valid in the concentration range where measurements were performed (Figure S2). Dark control samples of the SL-$MoS_2$ dispersion were covered by aluminum foil, illuminated, and analyzed in the same manner. The aggregation and sedimentation of SL-$MoS_2$ nanosheets under both dark and light conditions were investigated in the presence of SRNOM as described in Text S3 of Supporting Information.

## RESULTS AND DISCUSSION

### Structural Characterization and Colloidal Properties of $MoS_2$ Nanosheets.

Dispersions of SL-$MoS_2$ nanosheets were prepared via chemical exfoliation of $MoS_2$ powder following a method published previously.[13,43] The morphology of $MoS_2$ nanosheets was determined by TEM and AFM imaging. A typical TEM image of the exfoliated SL-$MoS_2$

nanosheets (Figure 1a) reveals thin flakes with lateral dimensions between 100 and 300 nm, consistent with the reported size of monolayer $MoS_2$.[46] The $z$-average $D_h$ of the SL-$MoS_2$ nanosheets obtained from three replicates was 230 ± 6 nm as determined by DLS (Figure 1b). Analysis of AFM images (Figure 1c) shows that the typical thickness of $MoS_2$ nanosheets is ~1.2 nm, confirming the preparation of monolayer $MoS_2$ without surface coatings.[46] The phase composition of $MoS_2$ nanosheets was determined semi-quantitatively by XPS. The Mo 3d spectrum of $MoS_2$ nanosheets (Figure 1d) reveals the coexistence of 1T- and 2H-$MoS_2$ in the exfoliated samples, which was caused by the partial phase conversion from 2H-$MoS_2$ to 1T-$MoS_2$ during lithium intercalation.[6] Deconvolution of the XPS spectrum reveals the phase composition of SL-$MoS_2$ to be 70% 1T and 30% 2H, in agreement with the reported composition of chemically-exfoliated monolayer $MoS_2$.[47]

The exfoliated SL-$MoS_2$ nanosheets were negatively charged with apparent zeta potentials of –37 to –40 mV in the pH range from 4 to 11 (Figure 1e), indicating excellent colloidal stability of $MoS_2$ nanosheet suspension. The negative charge on the exfoliated SL-$MoS_2$ reportedly stems from electron transfer from the organolithium reagent during the exfoliation process and is in the range of approximately 0.15 to 0.25 electron per Mo atom.[48] Under more acidic conditions (pH < 4), however, the apparent zeta potential decreased to –26 mV and rapid aggregation ensued due to the reduction of electrostatic repulsive force between the nanosheets.[48] The UV-vis absorption spectra of SL-$MoS_2$ (Figure 1f) is featureless without apparent absorption bands, consistent with metallic 1T-$MoS_2$ dominating the composition. At pH 6, $MoS_2$ nanosheets remained well-dispersed at least for one week in air although the absorbance of the dispersion decreased slightly due to oxidation of $MoS_2$ to soluble Mo(VI) (Figure 1f).[43] Oxidation of SL-$MoS_2$ nanosheets would not alter colloidal stability unless adequate $H^+$ was released to reduce the solution pH below

4.[43] The as-prepared SL-$MoS_2$ was stored in a $N_2$-filled glove box until further experimentation. Under these conditions, the suspension was stable for at least six months and no oxidation was observed. Considering the typical range of pH values in natural aquatic environments, pH variation alone would not destabilize SL-$MoS_2$ nanosheets, and colloidal stability can be maintained for long-term transport and exposure in the absence of the effects of co-occurring cations and/or light (see below).

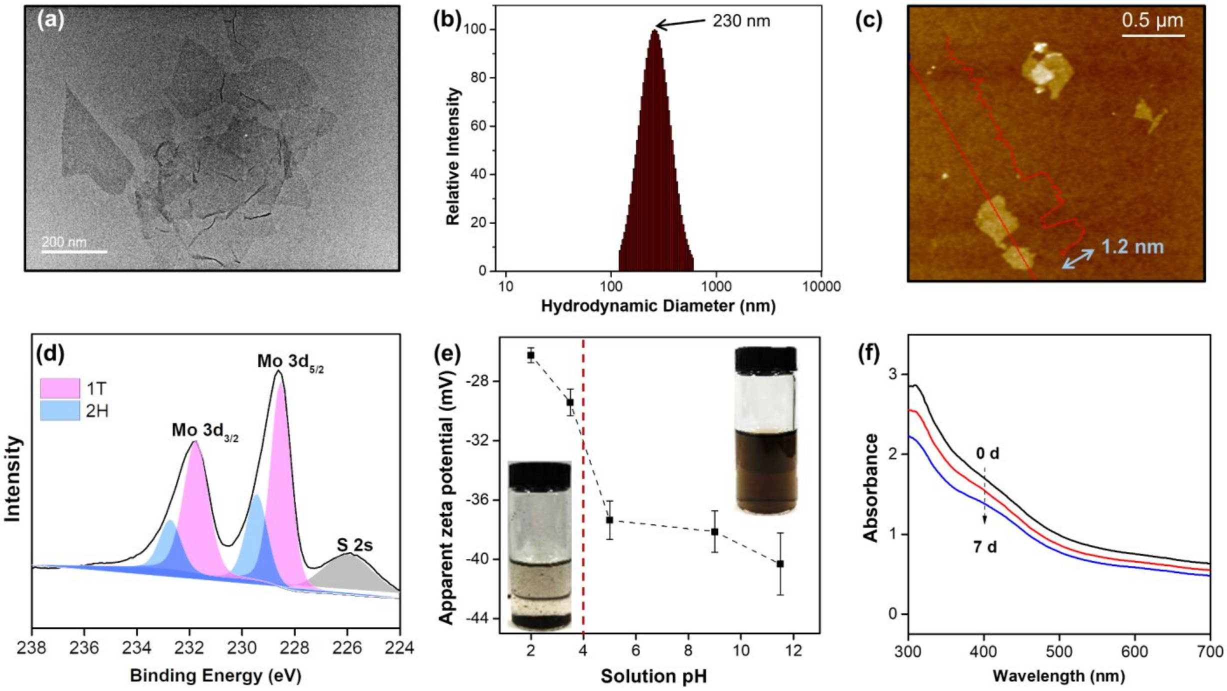

**Figure 1.** Characterization of SL-$MoS_2$ dispersion: (a) representative TEM image; (b) z-averaged hydrodynamic diameter distribution determined by DLS; (c) representative AFM image of $MoS_2$ nanosheets, inset: line scan showing the thickness profile along the red line in the image; (d) Mo 3d XPS spectra of SL-$MoS_2$ showing the deconvolution of two components: metallic 1T phase (pink) and semiconducting 2H phase (blue); (e) apparent zeta potential as a function of pH with photographs of as-prepared $MoS_2$ dispersion showing poor stability with aggregates at pH 2 (left) and good colloidal stability at pH 9 (right); (f) time-dependent UV-vis absorbance spectra for a $MoS_2$ dispersion over 7 d.

**Cation-induced Aggregation and Sedimentation of SL-$MoS_2$.** Figure 2 visually demonstrates the colloidal stability of SL-$MoS_2$ suspensions in the presence of varying concentrations of different metal cations (as nitrate salts) after 24 h. At low electrolyte concentration, the dispersion was homogenous with a dark brown color, implying good colloidal stability of SL-$MoS_2$ nanosheets. The suspension became colloidally unstable with the formation of large visible aggregates when the electrolyte concentrations were increased to specific levels, which appeared to depend on the type of cation (i.e., 10 mM for $Na^+$, 10 mM for $K^+$, 0.2 mM for $Ag^+$, 0.2 mM for $Ca^{2+}$, 0.2 mM for $Mg^{2+}$, 0.2 mM for $Cd^{2+}$, 0.1 mM for $Pb^{2+}$ and 0.05 mM for $Cr^{3+}$). Generally, the efficiency of the electrolytes in destabilizing $MoS_2$ nanosheets follows the order of trivalent > divalent > monovalent, suggesting stronger destabilization ability of cations with higher valency.

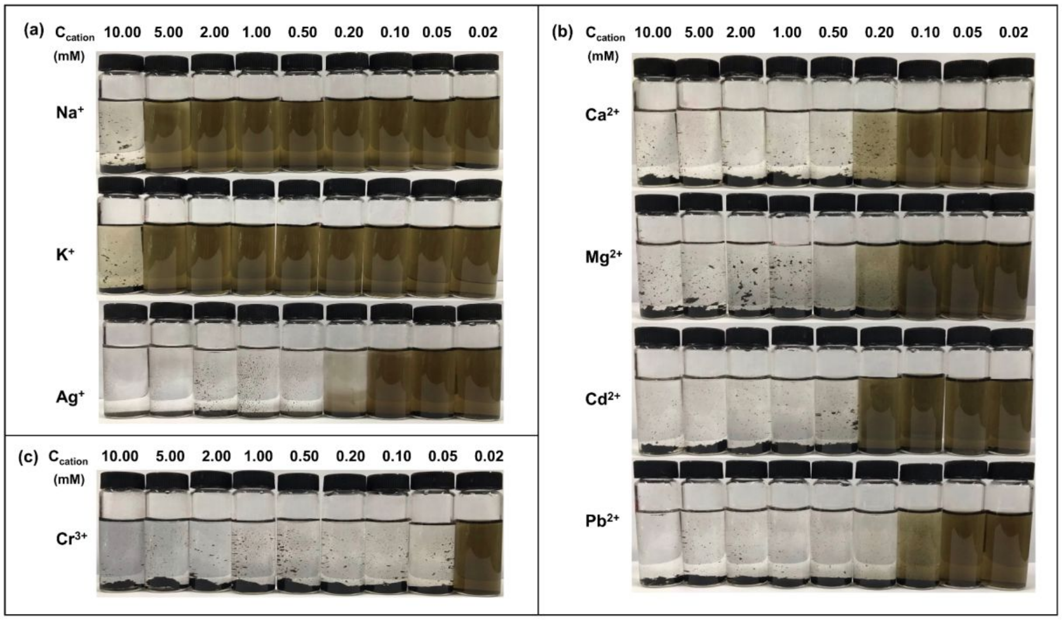

**Figure 2.** Images illustrating the bulk aggregation of SL-$MoS_2$ dispersions containing (a) monovalent, (b) divalent and (c) trivalent cations in a series of concentrations (0.02-10 mM).

To describe the aggregation kinetics more quantitatively, $D_h$ was experimentally determined as a function of cation concentration. Figure 3a shows such data for $Ca^{2+}$. Corresponding data for the other cations investigated (viz. $K^+$, $Na^+$, $Ag^+$, $Mg^{2+}$, $Cd^{2+}$, $Pb^{2+}$, and $Cr^{3+}$) are shown in Figure S3. The $D_h$ increased more rapidly at higher cation concentration due to charge screening or electrical double layer (EDL) compression, leading to rapid aggregation of the nanosheets. Attachment efficiency (α) was estimated by normalizing initial aggregation rate with that at the fast regime, and plotted in a log-log format as functions of concentrations of each cation. Consistent with classical DLVO theory, these plots exhibit reaction-limited and diffusion-limited aggregation regimes for $MoS_2$ nanosheets, and the transition between two regimes is referred to as the CCC value, the minimum concentration of ions necessary to cause rapid coagulation of colloids (Figure 3b). Starting from pure water, the energy barrier for attachment is reduced (as reflected in the increase in attachment efficiency) as the cation concentration increases up to the CCC (0.97 mM in the case of $Ca^{2+}$) at which point it vanishes. At electrolyte concentrations exceeding the CCC, SL-$MoS_2$ aggregation is limited by thermal diffusion rather than surmounting the repulsive energy-barrier, and thus aggregation rate becomes independent of cation concentration. The CCC values of SL-$MoS_2$ for the cations investigated are estimated to be 49 ± 7.2 mM ($K^+$), 28 ± 5.5 mM ($Na^+$), 0.20 ± 0.04 mM ($Ag^+$), 0.97 ± 0.04 mM ($Ca^{2+}$), 0.8 ± 0.20 mM ($Cd^{2+}$), 0.8 ± 0.1 mM ($Mg^{2+}$), 0.07 ± 0.001 mM ($Pb^{2+}$) and 0.05 ± 0.02 mM ($Cr^{3+}$) (Figure 3b). The CCC values of SL-$MoS_2$ are lower than those of black phosphorous[23] (188.4 mM for $Na^+$, 2.5 mM for $Ca^{2+}$) and GO[49] (188 mM for $Na^+$, 2.9 mM $Ca^{2+}$) although they possess similar apparent zeta potentials, which may be attributed to the stronger van der Waals (vdW) forces between $MoS_2$ nanosheets. Molybdenum disulfide has a Hamaker constant of $296\times10^{-21}$ J while that of GO is $49\times10^{-21}$ J.[25,50] To the best of our knowledge, this is the first report of CCC values for bare monolayer $MoS_2$ nanosheets. Higher CCC values (37 mM $Na^+$, 3 mM $Ca^{2+}$) were seen in the case of ethanol-coated few-layer $MoS_2$ prepared via ultrasonic exfoliation,[25] indicating that bare $MoS_2$ nanosheets in our study are more prone to aggregation. Applications are likely to employ surfactant- or coating-free $MoS_2$ for optimized catalytic, adsorptive, and conductive properties. The aggregation behavior of surface-coated $MoS_2$ might not represent that of the material itself because surface coatings may conceal $MoS_2$ surface properties associated with aggregation behavior and stabilize the nanosheets through additional steric repulsion.

Generally, the CCC values of multivalent cations were significantly lower than those of the monovalent cations (with exception of $Ag^+$), indicating that multivalent electrolytes destabilize SL-$MoS_2$ suspensions more effectively than monovalent electrolytes. Similar trends were observed in previous reports on the aggregation of other nanomaterials including some nanosheets such as GO[22,49,51], MXene[24], black phosphorous[23], consistent with the applicability of DLVO theory in predicting the general aggregation behavior of 2D nanomaterials. The lower CCC values for multivalent relative to the monovalent cations are in accordance with the Schulze-Hardy rule ($\log(\mathrm{CCC}) = n \log(\frac{1}{z})$), where $z$ is the valency of the electrolyte counterions and $n$ is constant, typically 6 in 3D and 9 in 2D aggregation.[26,52] A slope of –5.98 was obtained by the best fitting ($R^2 = 0.98$) for these CCC values of cations with exception of $Ag^+$ and $Pb^{2+}$ (Figure 3c). The valency exponent of 6.0 is commonly found in the aggregation of colloidal particles and suggests that cation-induced aggregation of SL-$MoS_2$ is a random process likely leading to edge-to-face interactions rather than solely face-to-face interaction which, based on theory, is expected to lead to an exponent of 9. The randomness of aggregation was evidenced from the TEM (Figure 3d) and SEM (Figure S4a) images of the sphere-like aggregates formed in the SL-$MoS_2$ dispersion containing 2 mM $Ca^{2+}$. For comparison, we prepared aligned stacks by filtration of SL-$MoS_2$ suspension through a polymer substrate (Figure 3e) as demonstrated by cross-sectional SEM (Figure S4b). The random and aligned configurations were qualitatively confirmed by XRD. As shown in XRD spectra (Figure 3f), the peak of aligned $MoS_2$ stacks was located at $2\theta = 14°$, corresponding to the characteristic interlayer spacing between neighboring layers of 0.62 nm.[8,53]

In contrast, the XRD peak of the cation-induced aggregates of $MoS_2$ mostly disappeared due to the disorder structure in the randomly aggregated sample.

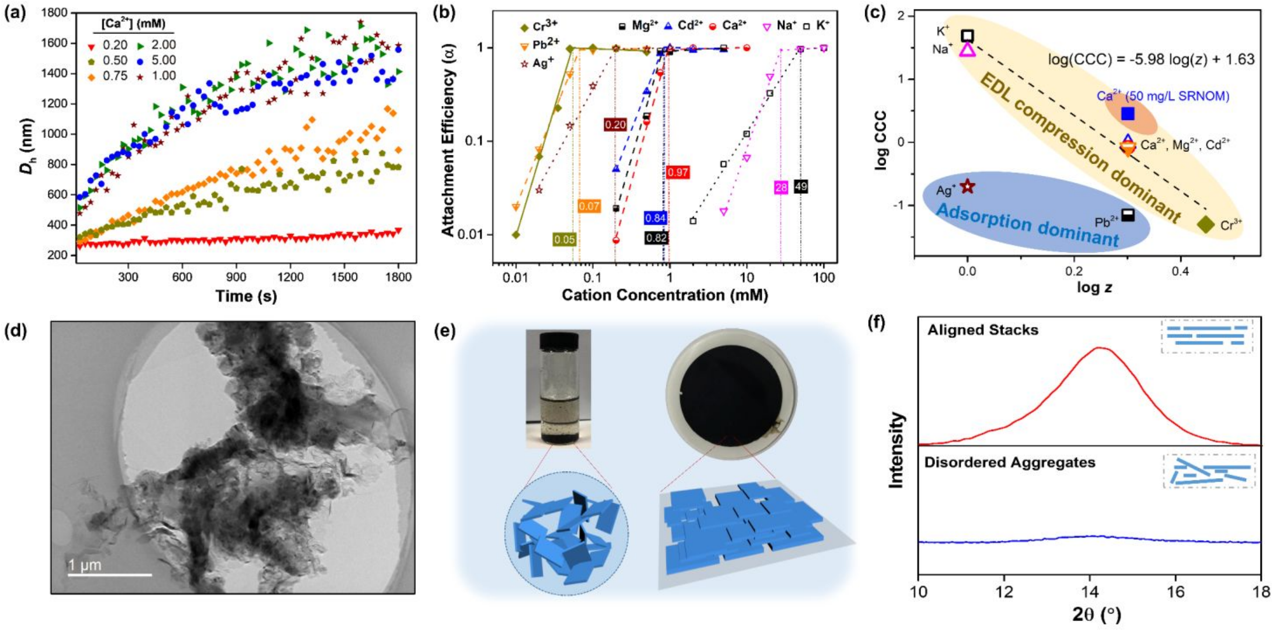

**Figure 3.** Effects of cation type and concentration on $MoS_2$ nanosheet aggregation: (a) changes in hydrodynamic diameter ($D_h$) over 30 min after addition of $Ca^{2+}$ (0.02-10 mM); (b) attachment efficiency (α) as a function of the concentrations of the indicated cations; (c) relationship between the critical coagulation concentration (CCC) and cation valence (*z*); (d) TEM image of $MoS_2$ aggregates formed in the presence of 2 mM $Ca^{2+}$; (e) photographs and schematic illustration of disordered aggregates (left) and face-to-face aligned stacks (right); (f) X-ray diffractograms of $MoS_2$ aggregates and aligned stacks.

For the cations with equivalent valency, the CCC values were ranked as $K^+ > Na^+ >> Ag^+$ and $Ca^{2+} > Mg^{2+} \approx Cd^{2+} >> Pb^{2+}$. In general, the ordering within groups of cations with equivalent valency is inversely related to the electronegativity of the cation (Figure S5a). This is attributable to cations with higher electronegativities more easily forming covalent bonds with S, leading to stronger ability to destabilize dispersions of $MoS_2$ nanosheets.[54,55] We note that $Ag^+$ and $Pb^{2+}$ display much lower CCC values than other monovalent and divalent cations (Figure 3c). As reported previously, $Ag^+$ and $Pb^{2+}$, as soft Lewis acids, have high affinity to the soft Lewis base S atoms and are thus more strongly adsorbed to the $MoS_2$ surface than are the hard ($Na^+$, $K^+$, $Mg^{2+}$,

$Ca^{2+}$) and borderline ($Cd^{2+}$) cations.[12,13,56] Adsorption of $Ag^+$ and $Pb^{2+}$ ions to the $MoS_2$ nanosheets would decrease the surface charge and weaken the electrostatic repulsion between nanosheets. For cations with much weaker affinity to S, the aggregation was mostly induced by EDL compression (Figure S5b).

Dissolved natural organic matter is a ubiquitous constituent in natural waters. Typical dissolved NOM concentrations in fresh surface waters range from 2 to 30 mg/L.[57] We therefore examined the effect of a reference aquatic NOM sample (viz. SRNOM) over a similar concentration range on SL-$MoS_2$ nanosheet aggregation in the presence of $Na^+$ or $Ca^{2+}$ (Figure S6). The SRNOM significantly inhibited the cation-induced aggregation kinetics of SL-$MoS_2$ nanosheets. For instance, the initial aggregation rate in the 2 mM $Ca^{2+}$ solution decreased from 1.18 nm/s in the absence of SRNOM to 1.08, 1.01, 0.62 and 0.27 nm/s by 5, 10, 20 and 50 mg/L SRNOM, respectively. Similarly, the initial rate of $D_h$ growth in the 50 mM $Na^+$ solution was 0.83 nm/s and dropped to 0.12 nm/s in the presence of 2 mg/L SRNOM; no aggregation was observable at SRNOM concentrations of 5 mg/L or higher (Figure S5b). In the presence of 20 and 50 mg/L SRNOM, the CCC of $Ca^{2+}$ were elevated to 1.95 and 2.86 mM, respectively (Figure S7), which were obviously larger than that in the absence of SRNOM (0.97 mM) and falling above the line predicted by Schulze-Hardy rule (Figure 3c). In the presence of 0.1 mM $Ca^{2+}$, the apparent zeta potentials of the nanosheets were increased from $-19$ mV to $-30$ mV by the addition of 20 mg/L SRNOM, implying the association of NOM with $MoS_2$ nanosheets. We therefore ascribe SRNOM stabilization of the SL-$MoS_2$ nanosheet suspension primarily to steric and electrostatic stabilization by the coated NOM molecules, similar to prior reports on the influence of NOM on the aggregation of negatively charged gold nanoparticles,[58] black phosphorus[23] and GO[21]. In addition, the carboxylate groups of SRNOM electrostatically bind $Ca^{2+}$,[59] thereby decreasing the charge screening and enhancing the colloidal stability of SL-$MoS_2$.

**Influence of Visible Light Illumination.** To investigate the effect of visible light on $MoS_2$ nanosheet aggregation and sedimentation, experiments were conducted in 0.2 and 2.0 mM $Ca^{2+}$ solutions (i.e., below and above the CCC value for $Ca^{2+}$, respectively) in the dark and under visible light illumination. As shown in Figure 4a, the presence of 2.0 mM $Ca^{2+}$ induced minor aggregation of $MoS_2$ nanosheets in the dark within 20 min. In contrast, the $MoS_2$ nanosheets strongly aggregated under illumination and started to sediment, which suggested that visible light illumination dramatically accelerated the aggregation process. Due to the limitation of DLS (not applicable for aggregates > 2 μm), the fraction of $MoS_2$ remaining in the suspension was quantified using absorbance at 450 nm. The evolution of normalized suspension concentrations depended on electrolyte concentration. Fast aggregation and sedimentation were observed when the $Ca^{2+}$ concentration exceeded its CCC (Figure S8), which was in accord with results obtained via TRDLS and justified the reliability of absorbance on the sedimentation of SL-$MoS_2$.

The normalized concentration of SL-$MoS_2$ remaining in suspension under different conditions is shown in Figure 4b, and can be well fit ($R^2$>0.98) by the first-order decay equation: $dc/dt = -kc$, where $c$ is the normalized concentration of the SL-$MoS_2$ dispersion at time $t$ (h), and $k$ ($h^{-1}$) is the first-order rate constant. In the presence of 2.0 mM $Ca^{2+}$, $k$ was $1.52 \pm 0.07$ $h^{-1}$ under illumination, compared to a value of $0.09 \pm 0.02$ $h^{-1}$ in the dark, indicating that illumination significantly accelerated aggregation, increasing the rate constant by a factor of 17. The acceleration also occurred in the dispersion containing 0.2 mM $Ca^{2+}$, with the rate constants of $0.06 \pm 0.02$ $h^{-1}$ and $0.15 \pm 0.005$ $h^{-1}$ in the dark and under illumination, respectively. Even at much lower $Ca^{2+}$ concentrations (0.02 and 0.05 mM, Figure S9a), the hydrodynamic diameters of $MoS_2$

nanosheets increased from 230 to ~1000 nm under light exposure, whereas they remained almost constant in the absence of illumination. Without cation addition, no aggregation was observed under either dark or light conditions. The results suggested that cation and visible light acted synergistically to induce aggregation of SL-$MoS_2$. Similar light-accelerated aggregation was observed in the presence of other cations ($Na^+$, $Mg^{2+}$, $Cr^{3+}$ in Figure S9b), indicating the light-enhanced aggregation is not specific to $Ca^{2+}$ and occurs in the presence of all cations tested. Furthermore, illumination-promoted aggregation correlates positively with the intensity of visible light: more severe aggregation occurs as light intensity increases from 0 to 100 mW/cm$^2$ (Figure S9c). Light-enhanced aggregation could also be seen from significantly reduced $C_{1/2}$, the concentration of $Ca^{2+}$ at which the normalized $MoS_2$ concentration is reduced to half after 6 hours. The $C_{1/2}$ value of $Ca^{2+}$ for $MoS_2$ nanosheets is 0.11 mM under light, almost 300-fold lower than that in the dark condition (29 mM, Figure S9d). The lower $C_{1/2}$ indicated much higher ability for the cation to induce destabilization under visible light illumination,[50,60] and thus the results suggest that stability of $MoS_2$ dispersion would be much more easily disturbed at or near the surface of sunlit waters.

Because dissolved NOM is ubiquitous in natural aquatic ecosystems, we also investigated light-assisted aggregation of SL-$MoS_2$ nanosheets in the presence of SRNOM. As shown in Figure 4c, SRNOM stabilized suspensions of SL-$MoS_2$ nanosheets both in the dark and under visible light illumination. The nanosheet sedimentation rate constant $k$ decreased with increasing SRNOM concentration (Figure 4d). Comparison of the sedimentation rate constants in the presence of SRNOM in the dark and under illumination demonstrates that visible light illumination accelerates aggregation, even in the presence of SRNOM. The extent to which sedimentation was accelerated as expressed by the ratio of $k$ obtained under illumination to that in the dark ($k_{light}/k_{dark}$) remains almost constant over the SRNOM concentration range of 2 to 50 mg/L (Figure 4d). Overall, these results suggest that light-accelerated sedimentation occurs regardless of whether SRNOM is present.

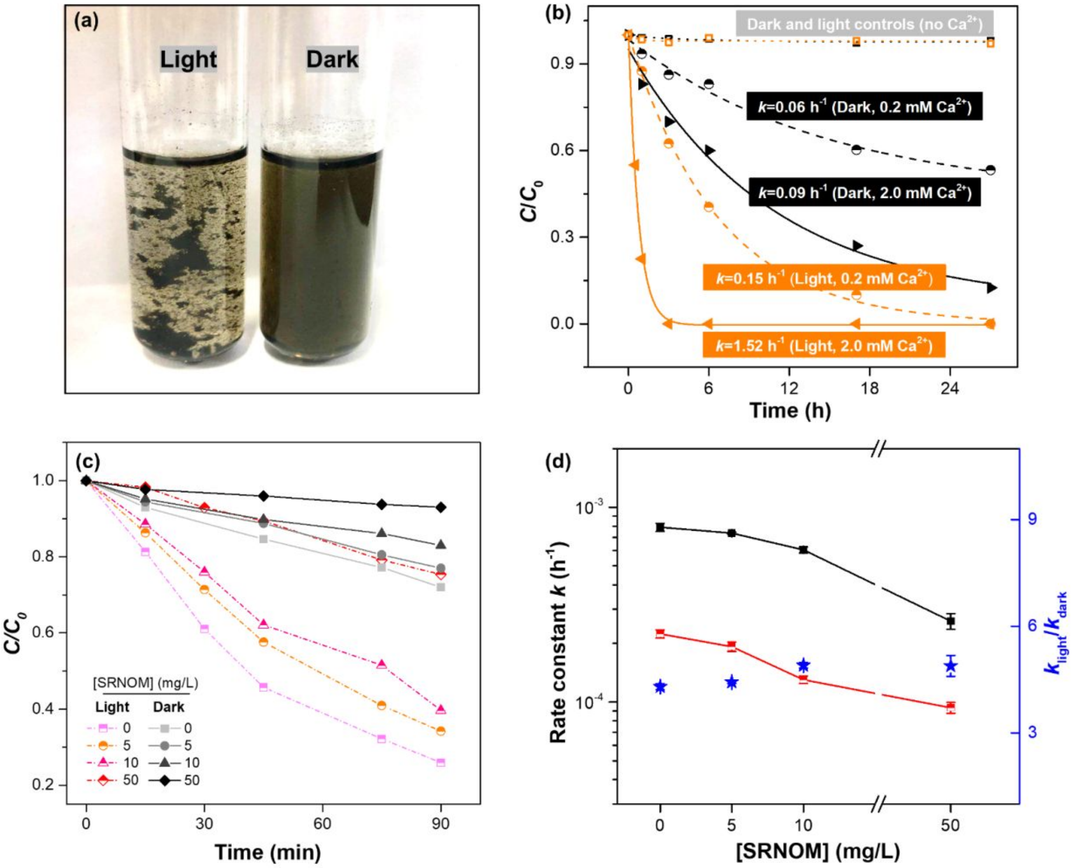

**Figure 4.** Accelerated aggregation and sedimentation of SL-MoS$_2$ dispersion under light irradiation: (a) digital photograph of SL-MoS$_2$ dispersion (~20 mg/L) with addition of 2.0 mM Ca$^{2+}$ after 20 min under illumination (left) and in the dark (right); (b) normalized suspension concentration as a function of time in the dark (solid lines) or under illumination (dashed lines) in the presence of 0.2 mM or 2.0 mM Ca$^{2+}$; (c) evolution of normalized suspension concentration in 2.0 mM Ca$^{2+}$ with addition of SRNOM in the dark (grey lines) or under illumination (colored lines); (d) sedimentation rate constants in the light (red) and dark (black). The ratios of $k$ in the light to that in the dark ($k_{light}/k_{dark}$) as a function of SRNOM concentration were represented by the blue stars.

**Light-accelerated Aggregation Mechanisms.** In the context of DLVO theory, light-enhanced aggregation of MoS$_2$ may be explained either by enhanced attractive vdW forces or by reducing electrostatic repulsion between neighboring nanosheets.[49,61] Diminished repulsive forces induced by photochemical reactions have been observed due to the reduction of surface charge in the cases of GO nanosheets under visible light illumination[38] and $TiO_2$ under UV irradiation,[39] or to the loss of surface coatings under irradiation in the cases of citrate-coated Ag nanoparticles[62] and functionalized/dispersant-coated SWCNT.[36,37,63] In the present case, we used bare $MoS_2$ without any surface functionalization. To test if illumination reduced electrostatic repulsion between SL-$MoS_2$ nanosheets, the dispersion was subjected to visible light illumination for 0.5, 2 or 10 h in the absence of $Ca^{2+}$ (referred to as irradiated $MoS_2$ and denoted $I_{0.5}$, $I_2$, or $I_{10}$). Electrolyte was then added, and aggregation kinetics was compared to that of pristine SL-$MoS_2$ in the dark and in the light. Figure 5a shows that aggregation kinetics differed to only a small extent between the pristine and light-exposed $MoS_2$ suspensions after addition of 2 mM $Ca^{2+}$ in the dark; in all cases aggregation was significantly slower than that when both $Ca^{2+}$ and light exposure were present simultaneously. This highlights the synergistic and indispensable roles of light and cations in accelerating the aggregation of SL-$MoS_2$ nanosheets.

In the absence of added metal cations, the apparent zeta potential of light-transformed $MoS_2$ remained largely unchanged ($p > 0.05$) after 10-hour irradiation (Figure S10). The XPS spectra revealed that the oxidation states of Mo and S reflected by their respect binding energies in the aggregates formed in light and dark were identical to those in pristine SL-$MoS_2$ (Figure S11). A prior study reported that long-term illumination (56 days) reduces the surface charge of SL-$MoS_2$ and thus destabilizes the dispersion.[18] In contrast, our results indicate that short-term visible light irradiation does not induce appreciable photochemical transformations of SL-$MoS_2$ that permanently alter the physiochemical properties of nanosheets to promote cation-triggered aggregation. Instead, a transient change of SL-$MoS_2$ nanosheets occurs under light irradiation, wherein the concurrent presence of electrolytes is required to induce the aggregation. Additionally, the temperature of irradiation solution was monitored during the test, and the variation was less than 2 °C. Accelerated aggregation due to solution heating by light irradiation was excluded by a control experiment, in which no obvious aggregation was observed in the presence of $Ca^{2+}$ when the temperature of the solution was elevated by 5 °C using a heating plate ($p > 0.05$; Figure S12).

A surface plasmon is a coherent oscillation of conduction band electrons at a metal/dielectric interface, a well-known mechanism of light-induced aggregation of Ag and Au nanoparticles as well as metallic carbon nanotubes.[40,41,64] In the case of SL-$MoS_2$, intercalation of Li/K partially transforms semiconducting 2H-$MoS_2$ to metallic 1T-$MoS_2$, creating more free charge carriers.[65] The adsorption for light was ascribed to interband transition and a surface plasmon for the semiconducting and metallic phase of $MoS_2$, respectively. Sufficient Li or K doping can achieve surface plasmon resonance under visible and near UV range.[33,34] To probe the relevance of the metallic phase in light-accelerated aggregation, the 1T-dominant SL-$MoS_2$ was converted to semiconducting 2H-$MoS_2$ nanosheets by a hydrothermal reaction without altering its monolayer morphology (Figure S13a). The 2H-$MoS_2$ nanosheets were comparable in size to the SL-$MoS_2$ nanosheets, with a hydrodynamic diameter of 277 ± 5 nm (Figure S13b). Apparent zeta potentials of 2H-$MoS_2$ dispersions were similar to those of SL-$MoS_2$ (Figure S13c), and thus the 2H-$MoS_2$ dispersion could remain colloidally stable for at least 3 days. The XPS spectrum demonstrated that the hydrothermally treated $MoS_2$ was pure 2H phase with typical 2H-Mo(IV) peaks at 229.3 and 232.4 eV (Figure S13d), and UV-vis absorption spectrum revealed the characteristic absorption bands of 2H-$MoS_2$ at 440, 610 and 670 nm,[43,47] distinct from the featureless absorption of pristine SL-$MoS_2$ (Figure 5b). The characterization above confirms the successful phase conversion and preservation of nanosheet morphology during hydrothermal treatment.

Regarding aggregation behaviors, Figure 5c shows similar and slow aggregation kinetics of the pristine SL-$MoS_2$ and the 2H-$MoS_2$ in the dark, confirming little variation of morphology or surface chemistry during phase conversion. Under visible light irradiation, however, the aggregation of 2H-$MoS_2$ is much less responsive to illumination, and the sedimentation accelerates to a smaller extent than that of SL-$MoS_2$ (Figure 5c). The results could be ascribed to that a larger amount of plasmonic electrons exists in the SL- than in the 2H-$MoS_2$ sample (Figure S14). We therefore confirmed the role of plasmonic electrons in aggregation in experiments using $Ag^+$ as electron scavengers.[66,67] In dark conditions, the sedimentation profile induced by 2 mM $Ca^{2+}$ was not influenced by inclusion of 20 μM $Ag^+$. This $Ag^+$ concentration is much lower than the CCC value for $Ag^+$ (200 μM). Under visible light irradiation, however, acceleration of aggregation was much less pronounced in the presence of $Ag^+$ (Figure S15a). This partial amelioration of aggregation was due to electrons scavenging by $Ag^+$ and resulted in the formation of $Ag^0$ (Figure S15b), supporting the role of plasmonic electrons in light-induced aggregation of $MoS_2$ nanosheets. The participation of electrons in light-enhanced aggregation was further demonstrated in aggregation experiments conducted in the absence or presence of molecular oxygen under illumination. Since oxygen can also serve as an electron scavenger, a further promoted aggregation was obtained as expected under oxygen-deficient conditions (Figure S15c).

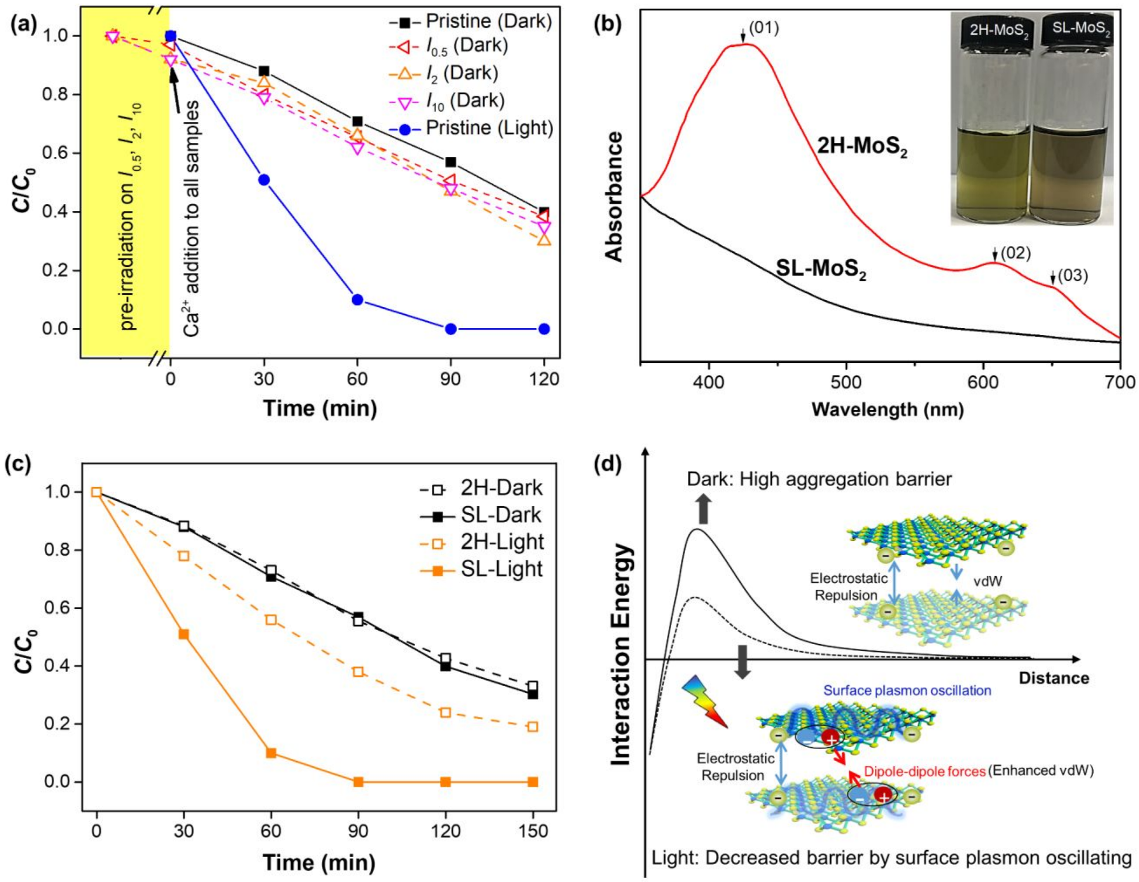

**Figure 5.** (a) Evolution of normalized SL-MoS$_2$ suspension concentrations and light-exposed MoS$_2$ (irradiated for 0.5 h, 2 h and 10 h in the absence of cations, referred to as $I_{0.5}$, $I_2$ and $I_{10}$, respectively) with addition of 2 mM Ca$^{2+}$ under dark or light irradiation; (b) UV−vis absorbance of pristine SL-MoS$_2$ (dark trace) and 2H-MoS$_2$ (red trace) with the characteristic peaks of the 2H phase marked by numbers. Inset: digital photographs of as-prepared 2H-MoS$_2$ (left) and pristine SL-MoS$_2$ (right) dispersions showing good colloidal stability; (c) Sedimentation of pristine SL-MoS$_2$ (solid lines) compared to 2H-MoS$_2$ (dashed lines) under dark (black) and light (orange) conditions; (d) Proposed mechanisms of aggregation under light and dark conditions.

Overall, the mechanisms of cation and visible light effects on the aggregation of SL-MoS$_2$ are proposed as shown in Figure 5d. In the dark, aggregation of SL-MoS$_2$ occurs upon addition of electrolytes through charge screening. Under illumination, surface conduction electrons in the metallic 1T-MoS$_2$ are excited and plasmon oscillation occurs on the nanosheet surface. When nanosheets approach closely enough for electromagnetic coupling, the optical spectra deviate from the Mie spectra, leading to the dipole induction in an electromagnetic field.[42] The plasmon dipole–

dipole interaction force correlates linearly with light intensity $E^2$ and dissipates as $h^{-4}$, in which $h$ denotes the separation distance, compared to the normal vdW force that dissipates as $h^{-7}$.[68] Hence, plasmon oscillation induces the generation of attractive forces between the nanosheets at longer distance than that occurs in the dark. Meanwhile, the classical DLVO theory describes the total interaction potential ($V_T$) of two colloidal particles by the sum of the vdW attractions ($V_{vdw}$) and the electric double layer repulsions ($V_{EDL}$):

$$V_T = V_{vdw} + V_{EDL}$$

Specifically, the $V_{vdw}$ between two flat surfaces expresses as: [69]

$$V_{vdw} = -\frac{AH}{12\pi d^2}$$

where $d$ is the sheet separation distance, $A$ is the surface area of the sheets, and $H$ is the Hamaker constant, resulting from zero-point fluctuations of electronic polarisations.[42] The value of $H$ is directly related to the dielectric permittivity, which would increase if the plasmonic materials including 1T-$MoS_2$ are excited by the incident light.[70] Excitation of these plasmons by absorbed light could therefore result in additional attractive forces via induced electromagnetic multipolar interactions,[42] decreasing the aggregation barrier between $MoS_2$ nanosheets at close approach. Clearly, the theoretical studies are required to better understand the mechanisms.

## ENVIRONMENTAL IMPLICATIONS

The potentially widespread application of TMDCs, especially $MoS_2$, has rendered the high necessity of research on the behaviors and stability in environment. In our study, pristine monolayer $MoS_2$ without surface coatings was chosen to reveal the intrinsic aggregation behaviors under environmentally relevant conditions. $MoS_2$ nanosheets behave similarly to most nanomaterials, tend to form aggregates and sediment in the presence of electrolytes *via* charge screening mechanism. However, the unique physiochemical properties and bare nanosheet surface lead to lower CCC values for $MoS_2$ nanosheets with common cations (e.g. $Na^+$, $Ca^{2+}$) and more easily destabilized suspensions in aquatic environments. The exposed sulfur atoms on $MoS_2$ nanosheets have high affinity to a variety of cations (e.g., Lewis soft acids $Pb^{2+}$) and mineral surfaces, the interactions of which may lead to their enhanced homoaggregation and heteroaggregation with other natural colloids in scenarios containing these species. At or near water surface, exposure to light irradiation can strongly enhance the aggregation kinetics though no appreciable photo-induced compositional changes occurred to the $MoS_2$ nanosheets. The presence of dissolved NOM sterically stabilized the $MoS_2$ nanosheets; nevertheless light-induced acceleration of aggregation was also operative in the presence of NOM. Our study implied the metallic 1T phase containing surface conducting electrons contributes to the transient surface plasmon oscillation, which leads to the accelerated aggregation in the presence of cations. Such a phase-dependent light-assisted aggregation mechanism is new and might happen in other 1T-dominant TMDCs, the phenomenon of which is particularly important as the metallic phase is favored in the applications of catalysis, energy storage, and contaminant remediation.[30,31] Given the enhanced aggregation in the interlayer of cation and light exposure, the actual aggregation and sedimentation at the natural water with sunlit could be substantial and thus the released $MoS_2$ are more likely existing as aggregates instead of 2D nanosheets. Effects of nanosheet aggregation and possible re-mobilization on the transport, exposure and toxicity to aquatic microorganisms should be considered in the future studies, in order to comprehensively understand the environmental fate and risks associated with $MoS_2$ and other TMDCs nanomaterials.

## ASSOCIATED CONTENT

### Supporting Information

Additional information on preparation of SL-$MoS_2$ nanosheets, supplementary aggregation results and characterization of 2H-$MoS_2$ is available in the Supporting Information. This material is available free of charge *via* the Internet at http://pubs.acs.org.

## ACKNOWLEDGEMENTS

This work was financially supported by the National Nature Science Foundation of China (Nos. 22076075 and 41907296). This work was also supported by SUSTech–MIT Joint Center for Mechanical Engineering Education and Research, and State Environmental Protection Key Laboratory of Integrated Surface Water-Groundwater Pollution Control. The authors acknowledge the assistance of SUSTech Core Research Facilities, and Dr. Dongsheng He for electron energy-loss spectroscopy characterization. The contributions of JAP were supported by the National Science Foundation under the Center for Sustainable Nanotechnology, CHE-2001611.

**Note:** the present address of JAP is Department of Environmental Health and Engineering, Johns Hopkins University, Baltimore, MD, 21218, United States.

## REFERENCES

(1) Wang, Z.; Zhu, W.; Qiu, Y.; Yi, X.; Von Dem Bussche, A.; Kane, A.; Gao, H.; Koski, K.; Hurt, R. Biological and Environmental Interactions of Emerging Two-Dimensional Nanomaterials. *Chem. Soc. Rev.* **2016**, *45* (6), 1750–1780.

(2) Bhimanapati, G. R.; Lin, Z.; Meunier, V.; Jung, Y.; Cha, J.; Das, S.; Xiao, D.; Son, Y.; Strano, M. S.; Cooper, V. R.; Liang, L.; Louie, S. G.; Ringe, E.; Zhou, W.; Kim, S. S.; Naik, R. R.; Sumpter, B. G.; Terrones, H.; Xia, F.; Wang, Y.; Zhu, J.; Akinwande, D.; Alem, N.; Schuller, J. A.; Schaak, R. E.; Terrones, M.; Robinson, J. A. Recent Advances in Two-Dimensional Materials beyond Graphene. *ACS Nano* **2015**, *9* (12), 11509–11539.

(3) Lembke, D.; Bertolazzi, S.; Kis, A. Single-Layer $MoS_2$ Electronics. *Acc. Chem. Res.* **2015**, *48* (1), 100–110.

(4) Liu, T.; Wang, C.; Gu, X.; Gong, H.; Cheng, L.; Shi, X.; Feng, L.; Sun, B.; Liu, Z. Drug Delivery with PEGylated $MoS_2$ Nano-Sheets for Combined Photothermal and Chemotherapy of Cancer. *Adv. Mater.* **2014**, *26* (21), 3433–3440.

(5) Midya, A.; Ghorai, A.; Mukherjee, S.; Maiti, R.; Ray, S. K. Hydrothermal Growth of Few Layer 2H-$MoS_2$ for Heterojunction Photodetector and Visible Light Induced Photocatalytic Applications. *J. Mater. Chem. A* **2016**, *4* (12), 4534–4543.

(6) Lukowski, M. A.; Daniel, A. S.; Meng, F.; Forticaux, A.; Li, L.; Jin, S. Enhanced Hydrogen Evolution Catalysis from Chemically Exfoliated Metallic $MoS_2$ Nanosheets. *J. Am. Chem. Soc.* **2013**, *135* (28), 10274–10277.

(7) Shi, Z. T.; Kang, W.; Xu, J.; Sun, Y. W.; Jiang, M.; Ng, T. W.; Xue, H. T.; Yu, D. Y. W.; Zhang, W.; Lee, C. S. Hierarchical Nanotubes Assembled from $MoS_2$-Carbon Monolayer Sandwiched Superstructure Nanosheets for High-Performance Sodium Ion Batteries. *Nano Energy* **2016**, *22*, 27–37.

(8) Wang, Z.; Tu, Q.; Zheng, S.; Urban, J. J.; Li, S.; Mi, B. Understanding the Aqueous Stability and Filtration Capability of $MoS_2$ Membranes. *Nano Lett.* **2017**, *17* (12), 7289–7298.

(9) Thurston, T. R.; Wilcoxon, J. P. Photooxidation of Organic Chemicals Catalyzed by Nanoscale $MoS_2$. *J. Phys. Chem. B* **1999**, *103* (1), 11–17.

(10) Liu, C.; Kong, D.; Hsu, P. C.; Yuan, H.; Lee, H. W.; Liu, Y.; Wang, H.; Wang, S.; Yan, K.; Lin, D.; Maraccini, P. A.; Parker, K. M.; Boehm, A. B.; Cui, Y. Rapid Water Disinfection Using Vertically Aligned $MoS_2$ Nanofilms and Visible Light. *Nat. Nanotechnol.* **2016**, *11* (12), 1098–1104.

(11) Fausey, C. L.; Zucker, I.; Lee, D. E.; Shaulsky, E.; Zimmerman, J. B.; Elimelech, M. Tunable Molybdenum Disulfide-Enabled Fiber Mats for High-Efficiency Removal of Mercury from Water. *ACS Appl. Mater. Interfaces* **2020**, *12* (16), 18446–18456.

(12) Wang, Z.; Tu, Q.; Sim, A.; Yu, J.; Duan, Y.; Poon, S.; Liu, B.; Han, Q.; Urban, J. J.; Sedlak, D.; Mi, B. Superselective Removal of Lead from Water by Two-Dimensional MoS2 Nanosheets and Layer-Stacked Membranes. *Environ. Sci. Technol.* **2020**, *54* (19), 12602–12611.

(13) Wang, Z.; Sim, A.; Urban, J. J.; Mi, B. Removal and Recovery of Heavy Metal Ions by Two-Dimensional $MoS_2$ Nanosheets: Performance and Mechanisms. *Environ. Sci. Technol.* **2018**, *52* (17), 9741–9748.

(14) Lowry, G. V.; Gregory, K. B.; Apte, S. C.; Lead, J. R. Transformations of Nanomaterials in the Environment. *Environ. Sci. Technol.* **2012**, *46*, 6893–6899.

(15) Hotze, E. M.; Phenrat, T.; Lowry, G. V. Nanoparticle Aggregation: Challenges to Understanding Transport and Reactivity in the Environment. *J. Environ. Qual.* **2010**, *39* (6), 1909.

(16) Mensch, A. C.; Hernandez, R. T.; Kuether, J. E.; Torelli, M. D.; Feng, Z. V.; Hamers, R. J.; Pedersen, J. A. Natural Organic Matter Concentration Impacts the Interaction of Functionalized Diamond Nanoparticles with Model and Actual Bacterial Membranes. *Environ. Sci. Technol.* **2017**, *51* (19), 11075–11084.

(17) Perreault, F.; De Faria, A. F.; Nejati, S.; Elimelech, M. Antimicrobial Properties of Graphene Oxide Nanosheets: Why Size Matters. *ACS Nano* **2015**, *9* (7), 7226–7236.

(18) Zou, W.; Zhou, Q.; Zhang, X.; Hu, X. Dissolved Oxygen and Visible Light Irradiation Drive the Structural Alterations and Phytotoxicity Mitigation of Single-Layer Molybdenum Disulfide. *Environ. Sci.*

*Technol.* **2019**, *53*, 7759–7769.

(19) Chng, E. L. K.; Sofer, Z.; Pumera, M. $MoS_2$ Exhibits Stronger Toxicity with Increased Exfoliation. *Nanoscale* **2014**, *6* (23), 14412–14418.

(20) Jeong, G. H.; Sasikala, S. P.; Yun, T.; Lee, G. Y.; Lee, W. J.; Kim, S. O. Nanoscale Assembly of 2D Materials for Energy and Environmental Applications. *Adv. Mater.* **2020**, *32* (35), 1–23.

(21) Chowdhury, I.; Duch, M. C.; Mansukhani, N. D.; Hersam, M. C.; Bouchard, D. Colloidal Properties and Stability of Graphene Oxide Nanomaterials in the Aquatic Environment. *Environ. Sci. Technol.* **2013**, *47* (12), 6288–6296.

(22) Yang, K.; Chen, B.; Zhu, X.; Xing, B. Aggregation, Adsorption, and Morphological Transformation of Graphene Oxide in Aqueous Solutions Containing Different Metal Cations. *Environ. Sci. Technol.* **2016**, *50* (20), 11066–11075.

(23) Tan, Z.; Yin, Y.; Guo, X.; Wang, B.; Shang, H.; Xu, J.; Zhao, Q.; Liu, J.; Xing, B. Natural Organic Matter Inhibits Aggregation of Few-Layered Black Phosphorus in Mono- and Divalent Electrolyte Solutions. *Environ. Sci. Nano* **2019**, *6* (2), 599–609.

(24) Xie, Y.; Gao, Y.; Ren, X.; Song, G.; Alsaedi, A.; Hayat, T.; Chen, C. Colloidal Behaviors of Two-Dimensional Titanium Carbide in Natural Surface Waters: The Role of Solution Chemistry. *Environ. Sci. Technol.* **2020**, *54* (6), 3353–3362.

(25) Mohona, T. M.; Gupta, A.; Masud, A.; Chien, S. C.; Lin, L. C.; Nalam, P. C.; Aich, N. Aggregation Behavior of Inorganic 2D Nanomaterials beyond Graphene: Insights from Molecular Modeling and Modified DLVO Theory. *Environ. Sci. Technol.* **2019**, *53* (8), 4161–4172.

(26) Li, B. L.; Zou, H. L.; Lu, L.; Yang, Y.; Lei, J. L.; Luo, H. Q.; Li, N. B. Size-Dependent Optical Absorption of Layered $MoS_2$ and DNA Oligonucleotides Induced Dispersion Behavior for Label-Free Detection of Single-Nucleotide Polymorphism. *Adv. Funct. Mater.* **2015**, *25* (23), 3541–3550.

(27) Lanphere, J. D.; Luth, C. J.; Guiney, L. M.; Mansukhani, N. D.; Hersam, M. C.; Walker, S. L. Fate and Transport of Molybdenum Disulfide Nanomaterials in Sand Columns. *Environ. Eng. Sci.* **2015**, *32* (2), 163–173.

(28) Wang, Z.; Mi, B. Environmental Applications of 2D Molybdenum Disulfide ($MoS_2$) Nanosheets. *Environ. Sci. Technol.* **2017**, *51* (15), 8229–8244.

(29) Bernardi, M.; Palummo, M.; Grossman, J. C. Extraordinary Sunlight Absorption and One Nanometer Thick Photovoltaics Using Two-Dimensional Monolayer Materials. *Nano Lett.* **2013**, *13* (8), 3664–3670.

(30) Acerce, M.; Voiry, D.; Chhowalla, M. Metallic 1T Phase $MoS_2$ Nanosheets as Supercapacitor Electrode Materials. *Nat. Nanotechnol.* **2015**, *10* (4), 313–318.

(31) Geng, X.; Sun, W.; Wu, W.; Chen, B.; Al-Hilo, A.; Benamara, M.; Zhu, H.; Watanabe, F.; Cui, J.; Chen, T. P. Pure and Stable Metallic Phase Molybdenum Disulfide Nanosheets for Hydrogen Evolution Reaction. *Nat. Commun.* **2016**, *7*, 1–7.

(32) Mak, K. F.; Lee, C.; Hone, J.; Shan, J.; Heinz, T. F. Atomically Thin $MoS_2$: A New Direct-Gap

Semiconductor. *Phys. Rev. Lett.* **2010**, *105* (13).

(33) Wang, Y.; Ou, J. Z.; Chrimes, A. F.; Carey, B. J.; Daeneke, T.; Alsaif, M. M. Y. A.; Mortazavi, M.; Zhuiykov, S.; Medhekar, N.; Bhaskaran, M.; Friend, J. R.; Strano, M. S.; Kalantar-Zadeh, K. Plasmon Resonances of Highly Doped Two-Dimensional $MoS_2$. *Nano Lett.* **2015**, *15* (2), 883–890.

(34) Habenicht, C.; Lubk, A.; Schuster, R.; Knupfer, M.; Büchner, B. Investigation of Potassium-Intercalated Bulk $MoS_2$ Using Transmission Electron Energy-Loss Spectroscopy. *Phys. Rev. B* **2020**, *101* (15), 155429.

(35) Kong, L.; Peng, X.; Hu, X.; Chen, J.; Xia, Z. UV-Light-Induced Aggregation of Arsenic and Metal Sulfide Particles in Acidic Wastewater: The Role of Free Radicals. *Environ. Sci. Technol.* **2018**, *52* (18), 10719–10727.

(36) Matsuzawa, Y.; Kato, H.; Ohyama, H.; Nishide, D.; Kataura, H.; Yoshida, M. Photoinduced Dispersibility Tuning of Carbon Nanotubes by a Water-Soluble Stilbene as a Dispersant. *Adv. Mater.* **2011**, *23* (34), 3922–3925.

(37) Chen, S.; Jiang, Y.; Wang, Z.; Zhang, X.; Dai, L.; Smet, M. Light-Controlled Single-Walled Carbon Nanotube Dispersions in Aqueous Solution. *Langmuir* **2008**, *24* (17), 9233–9236.

(38) Chowdhury, I.; Hou, W. C.; Goodwin, D.; Henderson, M.; Zepp, R. G.; Bouchard, D. Sunlight Affects Aggregation and Deposition of Graphene Oxide in the Aquatic Environment. *Water Res.* **2015**, *78*, 37–46.

(39) Sun, J.; Guo, L. H.; Zhang, H.; Zhao, L. UV Irradiation Induced Transformation of $TiO_2$ Nanoparticles in Water: Aggregation and Photoreactivity. *Environ. Sci. Technol.* **2014**, *48* (20), 11962–11968.

(40) Cheng, Y.; Yin, L.; Lin, S.; Wiesner, M.; Bernhardt, E.; Liu, J. Toxicity Reduction of Polymer-Stabilized Silver Nanoparticles by Sunlight. *J. Phys. Chem. C* **2011**, *115* (11), 4425–4432.

(41) Satoh, N.; Hasegawa, H.; Tsujii, K.; Kimura, K. Photoinduced Coagulation of Au Nanocolloids. *J. Phys. Chem.* **1994**, *98* (8), 2143–2147.

(42) Eckstein, H.; Kreibig, U. Light Induced Aggregation of Metal Clusters. *Zeitschrift für Phys. D Atoms, Mol. Clust.* **1993**, *26* (1), 239–241.

(43) Wang, Z.; Von Dem Bussche, A.; Qiu, Y.; Valentin, T. M.; Gion, K.; Kane, A. B.; Hurt, R. H. Chemical Dissolution Pathways of $MoS_2$ Nanosheets in Biological and Environmental Media. *Environ. Sci. Technol.* **2016**, *50* (13), 7208–7217.

(44) Wang, Z.; Zhang, Y. J.; Liu, M.; Peterson, A.; Hurt, R. H. Oxidation Suppression during Hydrothermal Phase Reversion Allows Synthesis of Monolayer Semiconducting $MoS_2$ in Stable Aqueous Suspension. *Nanoscale* **2017**, *9* (17), 5398–5403.

(45) Gueymard, C. A.; Myers, D.; Emery, K. Proposed Reference Irradiance Spectra for Solar Energy Systems Testing. *Sol. Energy* **2002**, *73* (6), 443–467.

(46) Lee, T. W.; Chen, C. C.; Chen, C. Chemical Stability and Transformation of Molybdenum Disulfide Nanosheets in Environmental Media. *Environ. Sci. Technol.* **2019**, *53* (11), 6282–6291.

(47) Guardia, L.; Paredes, J. I.; Munuera, J. M.; Villar-Rodil, S.; Ayán-Varela, M.; Martínez-Alonso, A.; Tascón, J. M. D. Chemically Exfoliated $MoS_2$ Nanosheets as an Efficient Catalyst for Reduction Reactions in the Aqueous Phase. *ACS Appl. Mater. Interfaces* **2014**, *6* (23), 21702–21710.

(48) Heising, J.; Kanatzidis, M. G. Exfoliated and Restacked $MoS_2$ and $WS_2$: Ionic or Neutral Species? Encapsulation and Ordering of Hard Electropositive Cations. *J. Am. Chem. Soc.* **1999**, *121* (50), 11720–11732.

(49) Wu, L.; Liu, L.; Gao, B.; Muñoz-Carpena, R.; Zhang, M.; Chen, H.; Zhou, Z.; Wang, H. Aggregation Kinetics of Graphene Oxides in Aqueous Solutions: Experiments, Mechanisms, and Modeling. *Langmuir* **2013**, *29* (49), 15174–15181.

(50) Gudarzi, M. M. Colloidal Stability of Graphene Oxide: Aggregation in Two Dimensions. *Langmuir* **2016**, *32* (20), 5058–5068.

(51) Gao, Y.; Chen, K.; Ren, X.; Alsaedi, A.; Hayat, T.; Chen, C. Exploring the Aggregation Mechanism of Graphene Oxide in the Presence of Radioactive Elements: Experimental and Theoretical Studies. *Environ. Sci. Technol.* **2018**, *52* (21), 12208–12215.

(52) Sano, M.; Kamino, A.; Shinkai, S. Critical Coagulation of Langmuir Monolayers : 2D Schulze - Hardy Rule. *J. Phys. Chem. B* **2000**, 10339–10347.

(53) Lu, X.; Gabinet, U. R.; Ritt, C. L.; Feng, X.; Deshmukh, A.; Kawabata, K.; Kaneda, M.; Hashmi, S. M.; Osuji, C. O.; Elimelech, M. Relating Selectivity and Separation Performance of Lamellar Two-Dimensional Molybdenum Disulfide ($MoS_2$) Membranes to Nanosheet Stacking Behavior. *Environ. Sci. Technol.* **2020**, *54* (15), 9640–9651.

(54) Lide, D. R. *CRC Handbook of Chemistry and Physics: A Ready-Reference Book of Chemical and Physical Data*; CRC press, 1995.

(55) Nieboer, E.; Richardson, D. H. S. The Replacement of the Nondescript Term ‘heavy Metals’’ by a Biologically and Chemically Significant Classification of Metal Ions.’ *Environ. Pollution. Ser. B, Chem. Phys.* **1980**, *1* (1), 3–26.

(56) Luo, J.; Fu, K.; Sun, M.; Yin, K.; Wang, D.; Liu, X.; Crittenden, J. C. Phase-Mediated Heavy Metal Adsorption from Aqueous Solutions Using Two-Dimensional Layered $MoS_2$. *ACS Appl. Mater. Interfaces* **2019**, *11* (42), 38789–38797.

(57) Wetzel, R. G. Limnology: Lake and River Ecosystems. In *San Diego: Elsevier Science & Technology*; San Diego: Elsevier Science & Technology: San Diego, 2001; pp 744–746.

(58) Louie, S. M.; Tilton, R. D.; Lowry, G. V. Effects of Molecular Weight Distribution and Chemical Properties of Natural Organic Matter on Gold Nanoparticle Aggregation. *Environ. Sci. Technol.* **2013**, *47* (9), 4245–4254.

(59) Christl, I. Ionic Strength- and PH-Dependence of Calcium Binding by Terrestrial Humic Acids. *Environ. Chem.* **2012**, *9* (1), 89.

(60) Guo, Y.; Deng, L.; Li, J.; Guo, S.; Wang, E.; Dong, S. Hemin-Graphene Hybrid Nanosheets with Intrinsic Peroxidase-like Activity for Label-Free Colorimetric Detection of Single-Nucleotide

Polymorphism. *ACS Nano* **2011**, *5* (2), 1282–1290.

(61) Baalousha, M. Effect of Nanomaterial and Media Physicochemical Properties on Nanomaterial Aggregation Kinetics. *NanoImpact* **2017**, *6*, 55–68.

(62) Mittelman, A. M.; Fortner, J. D.; Pennell, K. D. Effects of Ultraviolet Light on Silver Nanoparticle Mobility and Dissolution. *Environ. Sci. Nano* **2015**, *2* (6), 683–691.

(63) Hou, W. C.; He, C. J.; Wang, Y. S.; Wang, D. K.; Zepp, R. G. Phototransformation-Induced Aggregation of Functionalized Single-Walled Carbon Nanotubes: The Importance of Amorphous Carbon. *Environ. Sci. Technol.* **2016**, *50* (7), 3494–3502.

(64) Gopannagari, M.; Chaturvedi, H. Light Induced Aggregation of Specific Single Walled Carbon Nanotubes. *Nanoscale* **2015**, *7* (40), 16590–16596.

(65) Eda, G.; Yamaguchi, H.; Voiry, D.; Fujita, T.; Chen, M.; Chhowalla, M. Photoluminescence from Chemically Exfoliated $MoS_2$. *Nano Lett.* **2011**, *11* (12), 5111–5116.

(66) Yi, Z.; Ye, J.; Kikugawa, N.; Kako, T.; Ouyang, S.; Stuart-Williams, H.; Yang, H.; Cao, J.; Luo, W.; Li, Z.; Liu, Y.; Withers, R. L. An Orthophosphate Semiconductor with Photooxidation Properties under Visible-Light Irradiation. *Nat. Mater.* **2010**, *9* (7), 559–564.

(67) Chen, X.; Shen, S.; Guo, L.; Mao, S. S. Semiconductor-Based Photocatalytic Hydrogen Generation. *Chem. Rev.* **2010**, *110* (11), 6503–6570.

(68) Hallock, A. J.; Redmond, P. L.; Brus, L. E. Optical Forces between Metallic Particles. *Proc. Natl. Acad. Sci. U. S. A.* **2005**, *102* (5), 1280–1284.

(69) Israelachvili, J. N. *Van Der Waals Forces between Particles and Surfaces*; Academic press: Waltham, MA, 2011.

(70) Prieve, D. C.; Russel, W. B. Simplified Predictions of Hamaker Constants from Lifshitz Theory. *J. Colloid Interface Sci.* **1988**, *125* (1), 1–13.